Arch. Metall. Mater. **70** (2025), 3, 1081-1084

DOI: https://doi.org/10.24425/amm.2025.154446

YUJIN RHEE[1*], EQUO KOBAYASHI[1]

EFFECT OF COLD ROLLING ON PRECIPITATES EVOLUTION IN Al-5.5Zn-2.0Mg-2.4Cu ALLOY

In this work, the evolution and sequence of precipitates in a pre-deformed Al-Zn-Mg-Cu alloy during ageing were investigated by means of differential scanning calorimetry (DSC) measurements, scanning electron microscopy (SEM) and transmission electron microscopy (TEM). It was found that cold rolling alters the precipitation sequence due to the large density of deformation induced dislocations which were introduced during cold rolling, resulting in annihilation of excess vacancies and suppression of the formation of GP-zones. Also, large density of dislocations by cold rolling acts as heterogeneous nucleation sites for precipitates and then accelerated the formation of η precipitates making non-uniformly distributed size of precipitates either in matrix and grain boundary which strongly affects fracture surfaces.

Keywords: Aluminum alloy; Cold rolling (CR); Phase transformation; Precipitate evolution; Precipitation sequence

1. Introduction

7000 series Al-Zn-Mg-Cu alloys strengthened by artificial ageing (AA) are widely used in the aerospace and automotive industries due to light weight, high strength and good formability [1]. Generally, these excellent properties can be achieved by adjusting the parameters of not only typical heat treatment processes including solution heat treatment (SHT) followed by AA, but also more advanced thermo-mechanical treatment processes consisting different types of plastic deformation and heat treatment [2,3]. Thermomechanical treatments consisting of SHT, cold rolling (CR) and AA as a strengthening method in these age-hardenable Al alloys have been investigated by several groups [4-9]. In spite of the positive effects of CR, it has not been widely applied to the industrial fields because CR introduces deformation heterogeneity which means a non-uniform distribution of dislocations. This leads to inhomogeneous texture evolution and non-uniform distributions of macroscopic stress and strain. It was reported that pre-deformation before AA can alter the precipitation sequence [10-12]. Deschamps et al. [11] showed that the large density of dislocations introduced during plastic deformation alters the precipitation sequence. Allen et al. [13] and Deschamps et al. [14] found that in pre-deformed Al-Zn-Mg alloys, coarse equilibrium η phases preferentially formed on dislocations.

In the present study, the effects of cold rolling with different reduction ratios (30-90% reduction) on a precipitation evolutions and precipitation sequence of an Al-Zn-Mg-Cu alloy have been investigated by means of Differential scanning calorimetry (DSC), scanning electron microscopy (SEM) and transmission electron microscopy (TEM) and have clarified the type of precipitates and their behavior during ageing after cold rolling.

2. Experimental procedures

2.1. Materials and heat treatments

In this study, samples were 10 mm thick plates made from an Al-Zn-Mg-Cu alloy with a composition of Al-5.51Zn-1.99Mg-2.4Cu (wt.%). Samples were homogenized at 460°C for 6 h. Subsequently, we hot rolled each sample to a thickness of 50 mm to 10 mm. The samples were solution heat treated (SHT) at 480°C for 1 hour in a salt bath, followed by quenching in ice water. Immediately after SHT, the samples were cold-rolled at room temperature, reducing their thickness by 30%, 60%, and 90%. To maintain uniform deformation and minimize excessive temperature increases during cold rolling, each pass was limited to less than 10% thickness reduction. The samples were reduced

[1] TOKYO INSTITUTE OF TECHNOLOGY, DEPARTMENT OF MATERIALS SCIENCE AND ENGINEERING, TOKYO, JAPAN

* Corresponding author; rhee.y.aa@m.titech.ac.jp

from 1.5 mm to 1 mm in the '30%CR' condition, from 2.5 mm to 1 mm in the '60%CR' condition, and from 10 mm to 1 mm in the '90%CR' condition, respectively, with all samples ultimately adjusted to a thickness of 1 mm. Finally. The non-deformed and cold-rolled samples will be abbreviated as 'AQ,' '30%CR,' '60%CR,' and '90%CR,' respectively. Artificial aging (AA) was performed in an oil bath at 120°C for up to 14 days, depending on the initial condition

2.2. Differential scanning calorimetry (DSC), transmission electron microscopy (TEM) and scanning electron microscopy (SEM) measurements

DSC measurements were conducted using a Rigaku DSC8230 instrument in an argon atmosphere at a heating rate of 0.17K/s. The measurements were performed within the temperature range from –50°C to 500°C monitored by a liquid nitrogen controller. TEM specimens were obtained by grinding the samples from an initial thickness of around 1 mm down to 100 µm. Following this, 3 mm diameter discs were punched from the ground material. These discs were then electropolished using a Struers TenuPol-5 machine with an electrolyte mixture composed of one-third nitric acid (HNO_3) and two-thirds methanol (CH_3OH). During the electropolishing process, the electrolyte temperature was maintained between –20°C and –30°C. The TEM images were acquired using a JEOL 2100F microscope operated at 200 kV using. The fracture surfaces after the tensile tests were analyzed using a JEOL JSM-7200F field-emission scanning electron microscope (FE-SEM) operated at 15 kV.

3. Results and discussion

3.1. Phase evolutions by cold rolling ratios

Fig. 1 shows the DSC curves of 'AQ,' '30%CR,' '60%CR,' and '90%CR,' conditions. The DSC curves exhibit several peaks corresponding to precipitate nucleation and dissolution. For the AQ sample before ageing, two exothermic peaks appear at 107°C (peak A) and 232°C (peak C) while the exothermic peak B, is not observed. After 1 h ageing of AQ, peak A disappears. In CR samples with 30%, 60% and 90% reductions, it is observed that the exothermic peak (peak A) is very weak or almost negligible, while the second and third exothermic peak (shoulder peak B and peak C) appear in the temperature range of 170~220°C which is shifted to low temperature range compared to that of AQ sample. The shoulder peak B is more obvious when the cold rolling degree increases.

In the DSC curves (Fig.1) of the AQ sample, two sharp and clear exothermic peaks, A and C, associated with GP-zone formation at 107°C and η phase formation at 232°C are observed. Peak A disappears after short term ageing of 1 h, indicating that GP-zones form during the initial stages of AA and are responsible for the rapid age-hardening. For the CR samples, peak A is less prominent as compared to that of the AQ sample indicating that GP-zone formation is suppressed during subsequent ageing and the precipitation sequence may follow a different path, for example SSSS → η', η_2 due to accelerated formation of precipitates on dislocations. In the case of CR samples, excess vacancies are partly annihilated by deformation induced dislocations, suppressing the formation of GP-zones because dislocations serve as vacancy sinks. This leads to a reduction in the number of vacancies available for the formation of clusters and GP-zones [3,4,6]. Peak C is broadened and has a shoulder denoted B. The shoulder is more prominent as the cold rolling degree increases. A peak with a shoulder in DSC curves is probably due to different nucleation sites and/or morphology in the same phase formation [10]. Due to the non-uniform distribution of dislocations in the CR conditions, it is suggested that the peak with the shoulder is associated with formation of coarse precipitates nucleated on dislocations and fine precipitates nucleated in the matrix. Furthermore, the temperature related with η phase formation decreased with increasing CR ratios from 232°C for 90%CR to 227°C for AQ indicating that deformation induced dislocations act as heterogeneous nucleation sites for precipitates and accelerated the formation of η precipitates.

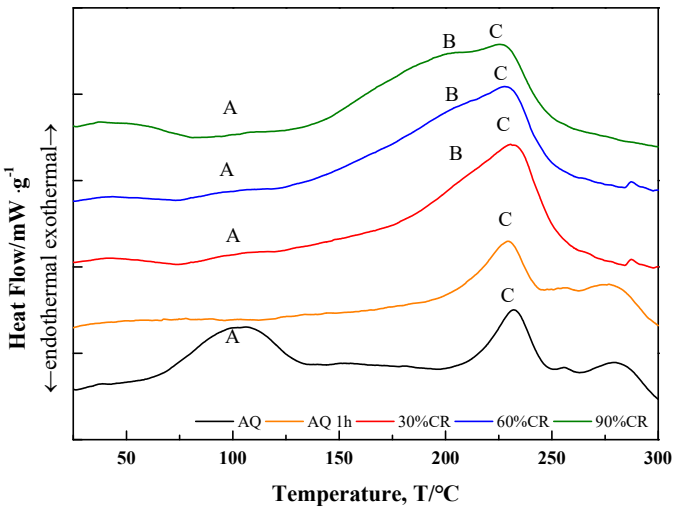

Fig. 1. DSC curves of AQ, AQ+1 h AA, 30%CR, 60%CR and 90%CR conditions

3.2. Precipitate evolution during ageing by cold rolling ratios

Fig. 2 shows bright-field (BF) TEM images of the AQ, 30%CR samples, 60%CR samples and 90%CR samples along the $<110>_{Al}$ zone axis. BF image of the AQ sample after ageing for 264 h at peak aged samples shows a uniform distribution of both plate-shaped and round-shape precipitates on $\{111\}_{Al}$ planes with an average size of approximately 5.5 nm in length and 2.2 nm in height based on 20 imaged precipitates shown in Fig. 2a. In Fig. 2b, BF TEM image of the 30%CR

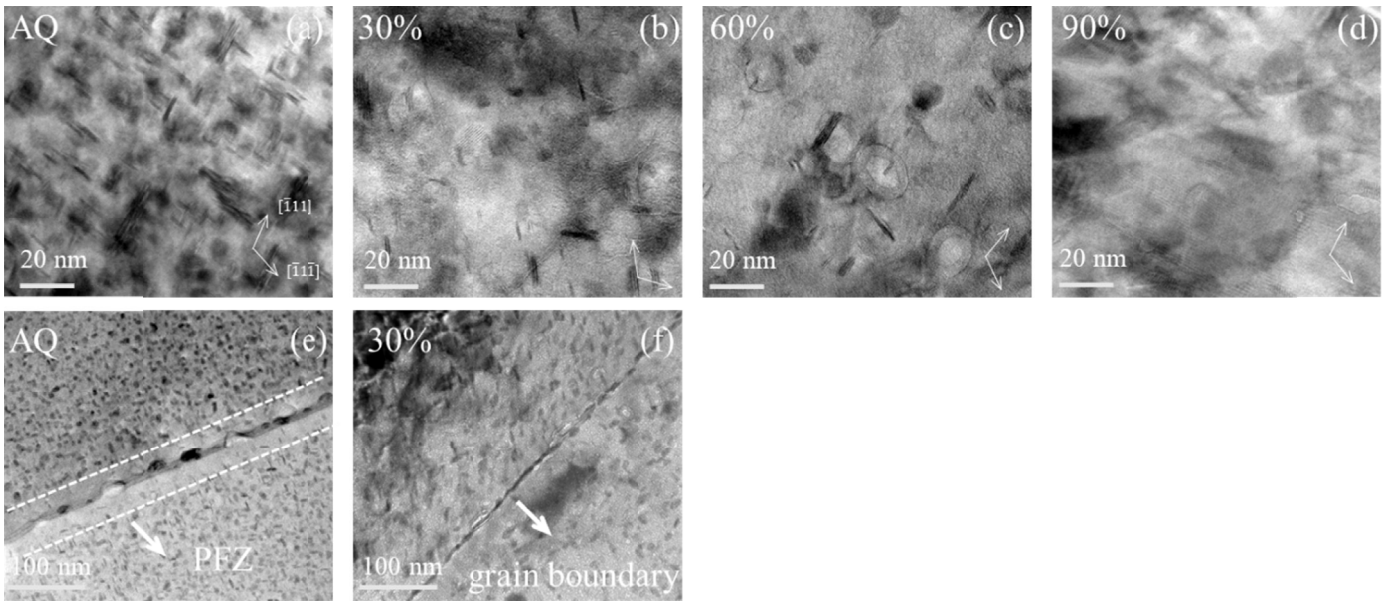

Fig. 2. BF image of the AQ sample ,30%CR sample, 60%CR sample and 90%CR sample aged at 120℃ for peak aged times viewed along <110> zone axes, (a)AQ for 264 h aged, (b) 30%CR for 18 h aged (c) 60%CR for 14 h aged (d) 90%CR for 14 h aged (e)AQ for 246 h at grain boundary region, (f) 30%CR for 18h at grain boundary region

sample at the peak-aged condition shows two different sizes of precipitates and significantly reduced numbers of precipitates. It is observed that precipitates with an average size of 8 nm in length and 3 nm in height regarded as η' or η_2 phase form in the matrix while precipitates with a size of 15 nm of length and 4 nm of height form on the deformation induced dislocations where nucleation and growth of precipitates are believed to be accelerated. Fig. 2c show BF TEM image of the 60%CR sample at the 14 h peak-aged condition. As in the case of the 30% CR sample, two types of precipitates were observed: small precipitates approximately 9 nm in size and larger ones around 18 nm. In addition, as the rolling reduction increased, the size of the precipitates tended to increase, while their total amounts of precipitates showed a decreasing. In the case of 90% CR samples, as shown in Fig. 2d, precipitates were not observed in the BF TEM images due to the high dislocation density. However, a significant number of dislocations remained even after the peak aged conditions.

At the grain boundary, precipitates free zone (PFZ) with a width of approximately 34 nm as shown in Fig. 2e. Fig. 2f shows a BF image of a grain boundary region of the 30%CR sample at the peak-aged condition. The PFZs are obviously narrow and not well developed in CR sample compared to AQ sample.

3.3. Fracture surface morphologies by cold rolling ratios

Tensile test results in this Al alloy by cold rolling ratios were previously reported by Rhee et al. [15] showing that the CR conditions showed higher mechanical strength than the AQ condition for all ageing times, and this effect increased with higher deformation ratios due to work hardening and that a higher age hardening response was observed for the AQ sample compared to that of the CR samples. Rhee et al. [15] also reported that the uniformly distributed SSSS containing high levels of quenched-in vacancies combined with negligible numbers of dislocations in the AQ sample enhanced precipitation of fine, homogeneous coherent/semi-coherent precipitates during ageing, while, in the CR samples, the pre-existing non-uniformly distributed dislocations lead to formation of coarser precipitates during ageing, having significantly reduced number densities as compared to the AQ condition.

Fig. 3a-h show the SEM fracture surface images of the AQ and CR samples both before ageing and at peak-aged conditions. In Fig. 3a, the fracture images of AQ exhibit significant and large deep dimples together with small dimples with 0.5 um size which represent ductile fractures with transgranular mode. The fracture surface at peak-aged condition shown in Fig. 3e is similar to the AQ sample before ageing but also shows dimples with intergranular mode as well as transgranular mode. This intergranular fracture mode is related with the softening of the grain boundaries having precipitation-free zones (PFZ) which decrease the strength of grain boundary. The fracture surfaces of 30% CR samples both before ageing and at peak-aged conditions are shown in Fig. 3b and Fig. 3f. In Fig. 3b and Fig. 3f, the shape and size of dimples of 30%CR sample show no significant difference from that of AQ. Therefore, fracture both of AQ and 30% CR conditions exhibit a ductile fracture with dimples having good ductility. 60%CR sample before ageing shows quasi-cleavage fracture mode but that of peak-aged condition shows mixed mode with quasi-cleavage fractures and ductile fracture with dimples shown in Fig. 3c, Fig. 3g1 and Fig. 3g2. This is consistent with the tensile test of 60%CR. The 90%CR samples in Fig. 3d and Fig. 3h shows quasi-cleavage fracture mode predominantly

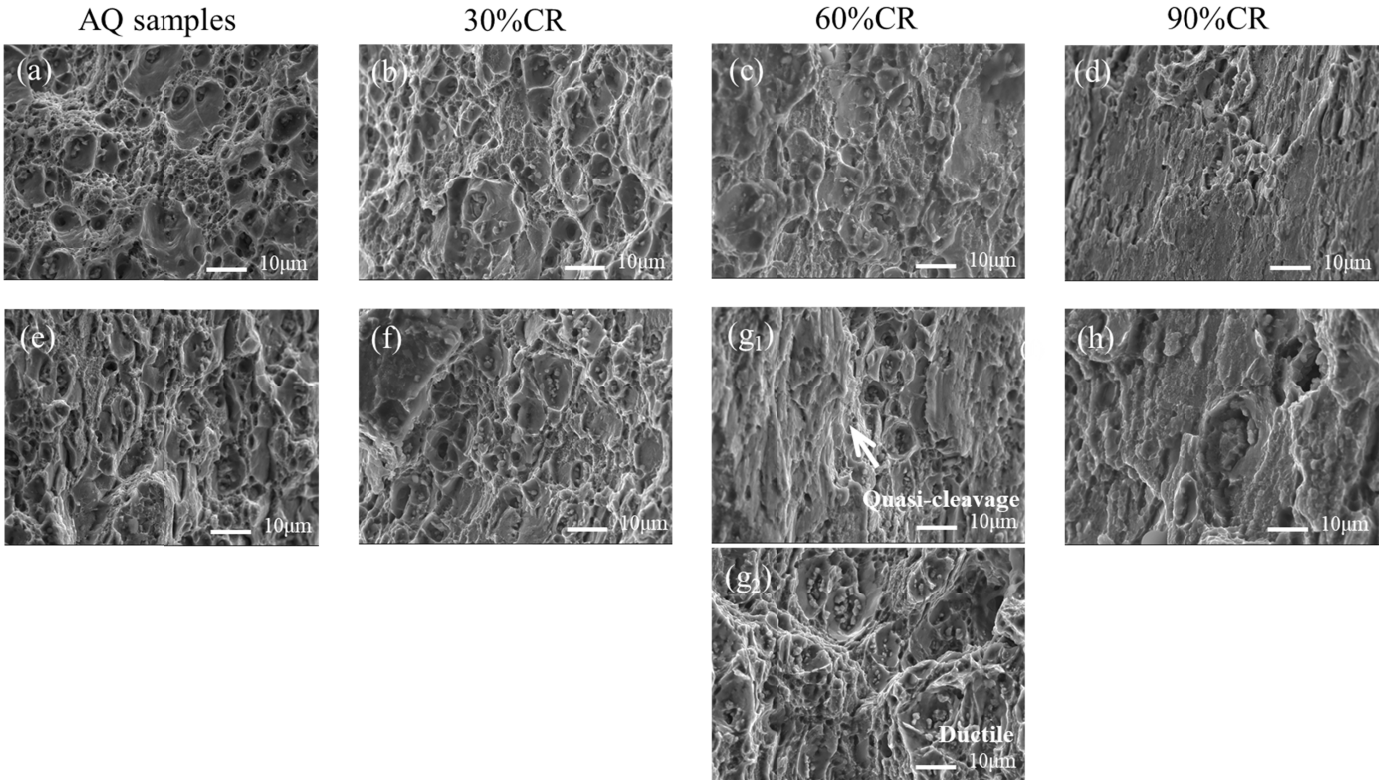

Fig. 3. Fracture surfaces of the AQ, 30%CR, 60%CR and 90% CR before ageing condition of (a)AQ, (b) 30%CR, (c) 60%CR, (d) 90%CR and peak aged condition of (e) AQ for 264 h, (f) 30%CR for 18 h, ($g_{1,2}$) 60%CR for 14 h (h) 90%CR for 14h

4. Conclusion

Pre-deformation introduced deformation heterogeneity in the Al matrix by large number of heterogeneous deformation induced dislocations during cold rolling and altered the precipitation sequence by means of annihilation of excess vacancies and suppression of the formation of GP-zones. Also, large density of dislocations by cold rolling serves as heterogeneous nucleation sites for precipitates and then accelerated the formation of η precipitates resulting in the formation of non-uniform coarse precipitates either in matrix and grain boundary which strongly affects fracture surfaces.

REFERENCES

[1] S. Li, X. Yue, Q. Li, H. Peng, B. Dong, T. Liu, H. Yang, J. Fan, S. Shu, F. Qiu, Q. Jiang, J. Mater Res. Tech. **27**, 944-983 (2023).

[2] C.H. Liu, X.L. Li, S.H. Wang, J.H. Chen, Q. Teng, J. Chen, Y. Gu, Mater. Design **54**, 144-148 (2014).

[3] D. Wang, Z. Ma, Z.M. Gao, Mater. Chem. Phys. **117**, 228-233 (2009).

[4] J. Huang, C. Xu, F. Jiang, Y. Jiang, Adv. Eng. Mater. **24**, 2100629 (2022).

[5] J.J. Xiao, C.Y. Liu, K. Cao, J. Mater. Eng. Perform. **33**, 1250-1261 (2024).

[6] C.D. Marioara, W. Lefebvre, S.J. Anderson, J, Friis, J. Mater. Sci. **48**, 3638-3651 (2013).

[7] R. Dai, K. Deng, C. Wang, K. Nie, C. Zhang, W. Liang, Mater. Sci. Eng. A **848**, 143388 (2022).

[8] H. Li, W. Xu, Z. Wang, B. Fang, R. Song, Z. Zheng, Mater. Sci. Eng. A, **650**, 254-263 (2016).

[9] T. Liu, H. Jiang, H. Sun, Y. Wang, Q. Dong, J. Zeng, F. Bian, J. Zhang, F. Chen, B. Sun, Mater. Sci. Eng. A **847**, 143342 (2022).

[10] A. Bendo, K. Matsuda, S. Lee, K. Nishimura, N. Nunomura, H. Toda, M. Yamaguchi. T. Tsuru, K. Hirayama, K. Shimizu, H. Gao, K. Ebihara, M. Itakura, T. Yoshida, S. Murakami, J. Mater. Sci. **53**, 4598-4611 (2018) .

[11] A. Deschamps, F. Livet, Y. Brechat, Acta Mater. **47**, 281-292 (1998).

[12] E. Thronsen, C.D. Marioara, J.K. Sunde, K. Minakuchi, T. Katsumi, I. Erga, S.J. Andersen, J. Friis, K. Marthinsen, K. Matsuda, R. Holmestad, Mater. Des. **186**, 108203 (2020).

[13] R.M. Allen, J.B. Vander Sande, Acta Metall. **28**, 1185-1195 (1980).

[14] A. Deschamps, Y. Brechet, P. Guyot, F. Livet, Zeitschrift für Metallkunde **88** (8), 601-606 (1997).

[15] Y. Rhee, E. Thronsen, O. Ryggetangen, C. D. Marioara, R. Holmested, E. Kobayashi, Met. Mater. Int. **30**, 3294-3310 (2024). DOI: https://doi.org/10.1007/s12540-024-01718-5